Journal of Materials and Manufacturing 5(2): 79-92 (2026)

Journal of Materials and Manufacturing

Comparative FEA of Static and Dynamic Structural Behavior in Low-Carbon Steel, Aluminum Alloy 6061, CFRP, and GFRP Bicycle Frames

Shamsher Khan[a,*], Shaukat Ali Shah[a], Hussain Ahmed[a]

[a]*Department of Mechanical Engineering, University of Engineering and Technology, Peshawar, Pakistan*
(ORCID:0009-0006-9575-3348), engrshamsherkhan12@gmail.com

(ORCID: 0000-0002-0297-2482), drsshah@uetpeshawar.edu.pk

(ORCID:0009-0002-0675-5490), Hussainahmed269@gmail.com

Abstract

Bicycle frames must balance strength, stiffness, weight, and cost, making material selection a central design decision. This study presents a comparative finite element investigation of four candidate frame materials - low-carbon steel, aluminum alloy 6061, carbon-fiber-reinforced polymer (CFRP), and glass-fiber-reinforced polymer (GFRP) - under static and dynamic loading. A sixteen-part CAD model of the frame, seat, and suspension system was built in Fusion 360 and analyzed in ANSYS Discovery under three static load cases (straight riding, 15° incline climbing, and 15° cornering), followed by time-domain multibody dynamic simulation in MSC Adams under two rider-load cases (1500 N and 900 N) with rotating wheel joints and wheel-ground contact forces. Under straight riding, Von Mises stress varied by less than 1.3% across materials (168.9–171.0 MPa), while total deformation scaled strongly with stiffness, ranging from 0.19 mm (steel) to 1.47 mm (GFRP) - roughly an eightfold spread. The 15° incline case produced the highest stresses of the three static scenarios, and under this case GFRP's Von Mises stress (259.2 MPa) exceeded its own yield strength (200 MPa), indicating a predicted yield exceedance that is not acknowledged in the underlying thesis. In the dynamic simulation, CFRP showed the largest load sensitivity, with stress falling from 120 MPa at 1500 N to 33 MPa at 900 N, while the source data contain an unresolved internal inconsistency between two dynamic-stress summary tables, which is reported rather than silently reconciled. Specific-stiffness and specific-strength calculations place CFRP well ahead of the other three materials, while steel remains the most predictable and cost-effective option. The findings support application-driven material selection - performance versus affordability versus terrain profile - rather than a single "best" material, and establish a baseline for future mesh-convergence, modal, and fatigue studies.

Keywords: Finite element analysis; bicycle frame; static structural analysis; dynamic analysis; ANSYS Discovery

1. Introduction

Bicycles remain one of the most widely used and affordable modes of transportation, particularly in developing regions, where they serve as a primary means of commuting, recreation, and fitness [1]. The global bicycle market was valued at USD 47.51 billion in 2019 and was projected to reach USD 59.27 billion by 2027, with the Asia-Pacific region - driven by population density, congested roads, and environmental concerns - holding the largest regional share; these market figures are reported here as motivating context from the source thesis's market study and were not independently re-verified for this manuscript. The frame is the structural skeleton that connects the seat, wheels, drivetrain, and handlebars, and it largely determines a bicycle's comfort, durability, and cost. Designing a frame that is simultaneously lightweight, durable, comfortable, and affordable

* Corresponding author
E-mail addresses: engrshamsherkhan12@gmail.com
DOI: 10.5281/zenodo.22775224
Received: 03 September 2026, Revised: 9 September 2026, Accepted: 15 September 2026
ISSN: 2822-6054 ©2026 The Author(s). Published by JMM under CC BY 4.0

is a genuine engineering trade-off, since improving one property frequently compromises another, and resolving that trade-off is fundamentally a materials-selection problem.

Static strength alone is an incomplete basis for frame design. A bicycle frame experiences vibration, shock, and cyclic loading from road irregularities, pedaling, and braking while in use, so its dynamic structural response - not only its behavior under a single static load - governs ride durability and rider safety. A material that performs acceptably under a static rider load can still behave very differently once time-varying wheel-contact forces and inertia are introduced, which is the motivation for pairing static FEA with a dynamic multibody simulation in this study.

Four materials were evaluated for their established relevance to frame design. Low-carbon steel is inexpensive, easy to manufacture, and mechanically reliable, and remains common in general-purpose frames. Aluminum alloy 6061 offers a favorable strength-to-weight ratio and good corrosion resistance and is widely used in performance-oriented frames. Carbon-fiber-reinforced polymer (CFRP) provides a very high strength-to-weight ratio and is used where weight reduction is paramount, such as in racing frames. Glass-fiber-reinforced polymer (GFRP) offers good corrosion resistance and electrical insulation at lower cost than CFRP, though with a substantially lower stiffness and yield strength. Finite element analysis (FEA) allows candidate materials and geometries to be screened computationally - predicting stress distribution, deformation, and (in a multibody context) dynamic response - before committing to physical prototyping, reducing development cost and iteration time.

Prior work has applied FEA and related numerical methods to individual aspects of bicycle-frame design: rapid prototyping and topology optimization of frame sections [2], static stress analysis of a bicycle frame in ANSYS [3], multiaxial fatigue design of welded frames [4], material and design studies of folding-bicycle frames [5], survey-based studies of rider comfort [6], reviews of bicycle dynamics and rider control [7], dynamic mechanical property analysis of electric-bike frames comparing steel, aluminum, and carbon fiber [8], and modal/harmonic response studies of frame structures [9]. Individually, these studies address either static structural behavior, fatigue, comfort, or dynamics - but rarely combine static and time-domain dynamic assessment of more than two or three materials under one consistent geometry and loading framework.

The present study addresses that gap by combining static structural FEA (ANSYS Discovery) with time-domain multibody dynamic simulation (MSC Adams) to compare four candidate frame materials - low-carbon steel, aluminum alloy 6061, CFRP, and GFRP - under a consistent frame geometry and a matched set of static and dynamic loading scenarios. To be explicit about scope: using FEA to evaluate individual bicycle-frame materials is well established in the literature reviewed above (Section 2), and this study does not claim a new analysis method. Its specific contribution is narrower and more concrete - evaluating four materials, including both metals and two polymer composites, on the same frame geometry under a combined static (three load cases) and time-domain dynamic (two load cases) framework, so that the resulting comparison is internally consistent rather than assembled from separate studies with different geometries and loading assumptions. The objective is therefore a systematic comparative numerical investigation that gives designers quantitative, side-by-side evidence for material choice under matched conditions, rather than a claim of a fundamentally new analysis method.

2. Literature Review

Collins et al. [2] combined fused deposition modeling with topology optimization to rapidly prototype a mountain-bike frame section, reporting an 18% weight reduction and a 12% stiffness increase relative to the original section - demonstrating the value of coupling numerical optimization with physical prototyping, though limited to a single material and section rather than a full-frame, multi-material comparison. Devaiah et al. [3] performed a CAD-based ANSYS stress analysis of a bicycle frame under various loading conditions, finding that the highest stress and deflection occurred at the frame joints and that stresses remained within allowable limits - a single-material static study that established joint regions as structurally critical, consistent with the load-path sensitivity observed in the present four-material comparison.

Callens and Bignonnet [4] evaluated the fatigue life of welded steel bicycle frames using a multiaxial fatigue criterion, finding it more accurate and conservative than a uniaxial criterion when compared against

experimental data. Their work highlights that static stress and deformation results, as reported in the present study, are not sufficient on their own to certify long-term durability - fatigue analysis is identified as a limitation and future-work item here for the same reason. Maleque et al. [5] compared steel, aluminum, and carbon fiber for folding-bicycle frames using ANSYS, proposing a design that balances strength, weight, and manufacturability. Their material set overlaps with the present study but was evaluated for a different frame typology (folding frames) and did not include a dynamic multibody assessment.

Ayachi et al. [6] surveyed 354 cyclists and found that bicycle comfort is shaped by both objective (frame/geometry) and subjective (rider preference, terrain) factors, underscoring that structural performance metrics such as stress and deformation are necessary but not sufficient for a complete frame-design evaluation. Schwab and Meijaard [7] reviewed bicycle dynamics and rider control, covering modeling, parameter identification, and stability - providing the broader dynamics context into which the present study's simplified rigid-body wheel/frame multibody model fits as a structural (not whole-vehicle stability) simulation. Iskandar et al. [8] used FEA to compare steel, aluminum, and carbon fiber electric-bike frames, reporting that carbon fiber gave the best strength, stiffness, and weight-reduction performance among the materials tested - a finding partially consistent with the present study's specific-stiffness and specific-strength results for CFRP, though obtained for a different (electric-bike) frame and loading context and without a GFRP comparison.

Sani et al. [9] conducted modal and harmonic-response analysis of a bicycle frame, identifying six natural frequencies and corresponding mode shapes and showing that excitation frequency and amplitude affect the harmonic response. This is the closest prior work to a true dynamic structural characterization, but it addresses natural-frequency/harmonic behavior rather than the time-domain, multibody, rolling-contact dynamic simulation performed here, and did not compare multiple candidate materials.

Outside the bicycle-frame literature specifically, two further studies inform the present analysis. Evran and Kurt [10] compared structural steel, aluminum alloy, magnesium alloy, and copper alloy plates under static compressive loading and topology optimization and found that total deformation varied much more strongly with material stiffness than did peak Von Mises stress - the same qualitative pattern observed here in Section 4.1, where Case 1 stress varies by only about 1.3% across four materials while deformation varies roughly eightfold. Şengül and Çalışkan [11], in a static FEA study of a steel hatch-ramp structure, computed a yield-strength-based safety coefficient directly from peak Von Mises stress - the same approach used to derive the static safety margins in Section 4.1 of this manuscript, and cited here as methodological precedent for that calculation.

Taken together, the literature has examined static stress analysis, fatigue, comfort, whole-vehicle dynamics, and modal response of bicycle frames, and has compared up to three candidate materials in a static or single-analysis-type context. What remains comparatively underexamined is a single, consistent frame geometry evaluated across four candidate materials under both static multi-case loading and time-domain multibody dynamic loading - the specific gap this study addresses.

3. Materials and Methods

3.1. Bicycle Frame Model

A sixteen-part three-dimensional CAD model of the bicycle frame, seat, and suspension system was developed in Fusion 360 (2023). Individual components were drawn to specified dimensions and assembled using the software's mate-tool mechanism (Fig. 1). The frame uses a lightweight, single-piece “biscuit-type” structural concept with a contoured seat and an under-seat spring-damper suspension intended to reduce transmitted vibration and shock to the rider. The completed assembly was exported in Parasolid format for import into ANSYS Discovery for static analysis, and in a compatible format for import into MSC Adams for dynamic simulation. Precise frame-tube dimensions, wheelbase, and head/seat-tube angles were not tabulated in the source thesis and are marked [information required]; only the assembled views in Fig. 1 are available. Reproducing this study, or comparing it against other frame designs, additionally requires tube outer diameters and wall thicknesses, cross-sectional shape at each joint, and full frame angle geometry - none of which is tabulated in the source thesis; these are listed explicitly here, rather than left as a general caveat, because they

materially affect the stress and deformation results and are needed before the results can be considered reproducible (see Section 5).

Fig. 1. CAD model of the frame, seat, and suspension assembly: (a) isometric, (b) side, (c) front view (Fusion 360).

3.2. Material Properties

Four materials were evaluated using the mechanical properties in Table 1, applied consistently across both the static and dynamic simulations. The source thesis also reports a qualitative comparison of corrosion resistance, fatigue resistance, weight-to-strength ratio, manufacturing complexity, cost, and typical applications for the same four materials (Table 1). This qualitative data is included because it is directly relevant to the cost/performance trade-offs discussed in Section 4.4, and it was not fabricated or estimated for this manuscript.

Table 1. Mechanical properties of the four candidate frame materials. Qualitative material comparison (corrosion resistance, fatigue resistance, weight-to-strength ratio, manufacturing complexity, and relative cost), reproduced from the source thesis.

Material	E (GPa)	Density (kg/m³)	Poisson's Ratio	Yield Strength (MPa)	Ultimate Strength (MPa)
Low-Carbon Steel	215	7990	0.30	430	600
Aluminum Alloy 6061	70	2800	0.33	300	320
CFRP	250	1820	0.21	1600	1820
GFRP	30	1800	0.32	200	250

Material	Corrosion Resistance	Fatigue Resistance	Weight-to-Strength Ratio	Manufacturing Complexity	Relative Cost
Low-Carbon Steel	Moderate	Moderate	Moderate	Low	Low
Aluminum Alloy 6061	Good	Good	High	Moderate	Moderate
CFRP	Excellent	Excellent	Very High	Moderate–High	High
GFRP	Good	Good	High	Moderate	Moderate

3.3. Finite Element Model and Mesh

Static analysis was performed in ANSYS Discovery, selected for its simplified, integrated interface and live-simulation feedback relative to the traditional ANSYS Workbench environment. The imported frame geometry was meshed using a combined tetrahedral and hexahedral sizing strategy intended to capture both the curved and flat surfaces of the frame, followed by mesh-quality checks. Exact element count, node count, element size, and a formal mesh-convergence study were not reported in the source thesis and are marked here as [information required]; a convergence study is recommended before journal submission (see Section 5).

3.4. Boundary Conditions and Loading

Static analysis (ANSYS Discovery) used three boundary-condition cases representing realistic riding scenarios: Case 1 - straight, level riding with no lateral or axial tilt; Case 2 - incline climbing, with a 15° tilt in the axial direction; and Case 3 - cornering, with a 15° tilt in the lateral-axial direction. In every case, fixed supports were applied at the rear dropout and bottom bracket, a rider load was applied at the seat/head-tube region, and gravity was included. Von Mises stress and total deformation were extracted as the primary response variables for all four materials in each case.

Fig. 2. Representative static boundary conditions (Case 1 shown): A/B fixed supports at rear dropout and bottom bracket, C free, D rider load, E gravity.

Dynamic analysis (MSC Adams) modeled the frame as a constrained rigid-body multibody system with revolute joints at both wheels (permitting anticlockwise rotation) and a sprocket joint at the central frame connection; contact forces were applied at the front and rear wheel-ground interfaces. Two loading scenarios were examined: Case 1 (maximum load) - 1500 N applied force, gravity of 9.8 m/s², wheel angular velocity of 100 RPM, and bicycle linear velocity of 3.5 m/s; and Case 2 (minimum load) - 900 N applied force, with gravity, angular velocity, and linear velocity unchanged from Case 1. Time-domain Von Mises stress and total deformation were recorded over approximately 0.2 s of simulated motion for each material and load case.

3.5. Static Analysis Procedure

For each of the four materials and three static load cases, ANSYS Discovery solved for the Von Mises equivalent stress field and total deformation field under the boundary conditions in Section 3.4. Peak Von Mises stress and peak total deformation were extracted for comparison across materials. Factor of safety was not explicitly computed in the source thesis; Section 4.1 of this manuscript derives an approximate static safety margin (yield strength / peak Von Mises stress) directly from Table 1 and the extracted stress results, and states this explicitly as a derived, not source-reported, quantity.

3.6. Dynamic Analysis Procedure

MSC Adams solved the time-domain equations of motion for the constrained rigid-body assembly under rolling ground contact, recording Von Mises stress and total deformation histories over the simulated 0.2 s window for each material and each of the two load cases. Both quantities showed oscillation and gradual damping over the first 0.1–0.15 s of simulated motion, consistent with transient settling of wheel rotation and rider load, before trending toward a steadier value. This is a rigid-body, time-domain dynamic simulation rather than a formal modal (natural-frequency) analysis; no modal analysis was performed in the source work despite being listed as a future-work item (Section 5). A further methodological gap concerns how structural stress and deformation were obtained at all: MSC Adams is fundamentally a multibody dynamics solver operating on rigid or (via Adams/Flex) flexible bodies, and the source thesis does not state whether Adams/Flex, a coupled external FEA solver, or another route was used to convert the multibody simulation into the reported Von Mises stress and deformation fields. This is marked [information required] and should be confirmed against the original Adams model files before the dynamic results in Section 4.2 are treated as final.

4. Results and Discussion

4.1. Static Structural Response

Table 2 reports Von Mises stress and total deformation for Case 1 (straight riding). Stress is nearly identical across the four materials (168.9–171.0 MPa, a spread of about 1.3%), indicating that stress magnitude in this load case is governed primarily by geometry and load path rather than material stiffness. Deformation, by contrast, scales strongly with material stiffness: low-carbon steel deflects only 0.19 mm, while GFRP deflects 1.47 mm - roughly eight times more, consistent with GFRP's much lower elastic modulus (30 GPa vs. 215 GPa for steel; Table 1) and with the general pattern reported by Evran and Kurt [10], who likewise found deformation far more material-sensitive than stress in a static plate-loading comparison across four metals.

Table 2. Static structural results - Case 1 (straight riding).

Material	Von Mises Stress (MPa)	Total Deformation (mm)
Low-Carbon Steel	170.98	0.19
Aluminum Alloy 6061	170.30	0.49
CFRP	169.61	0.84
GFRP	168.92	1.47

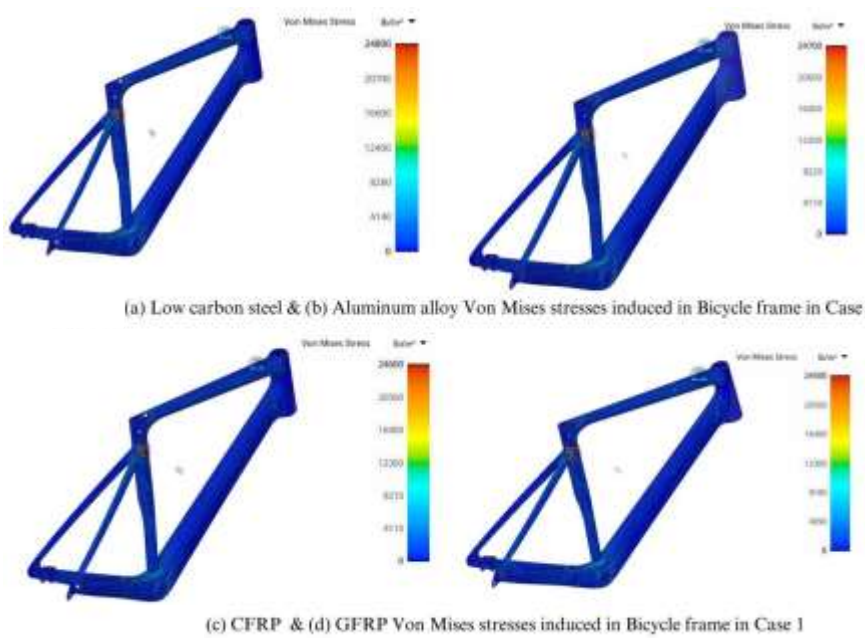

Fig. 3. Von Mises stress contours, Case 1: (a) steel, (b) aluminum 6061, (c) CFRP, (d) GFRP (ANSYS Discovery).

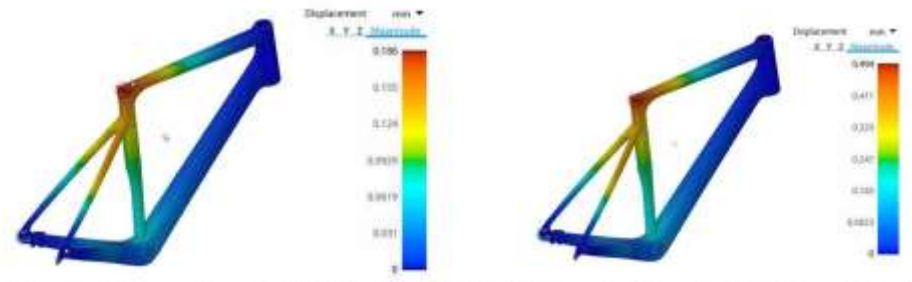

(a) Low carbon steel & (b) Aluminum alloy Total Deformation induced in Bicycle frame in Case 1

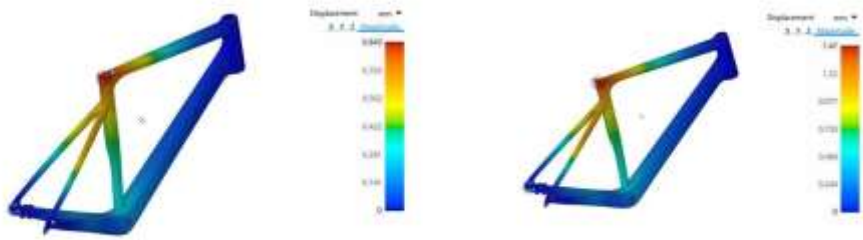

(c) CFRP & (d) GFRP Total Deformation induced in Bicycle frame in Case 1

Fig. 4. Total deformation contours, Case 1: (a) steel, (b) aluminum 6061, (c) CFRP, (d) GFRP (ANSYS Discovery).

Table 3 reports results for Case 2 (15° incline) and Case 3 (15° cornering). The incline case produces the highest stresses recorded across the three static scenarios, peaking at 272.34 MPa for CFRP. Cornering (Case 3) is the mildest of the three, with stresses roughly one-third those of the incline case.

Table 3. Static structural results - Case 2 (incline) and Case 3 (cornering).

Material	**Case 2**	**Case 2**	**Case 3**	**Case 3**
	Stress (MPa)	**Deformation (mm)**	**Stress (MPa)**	**Deformation (mm)**
Low-Carbon Steel	235.11	0.18	75.15	0.11
Aluminum Alloy 6061	227.52	0.50	73.00	0.29
CFRP	272.34	0.58	86.18	0.35
GFRP	259.24	1.45	82.00	0.89

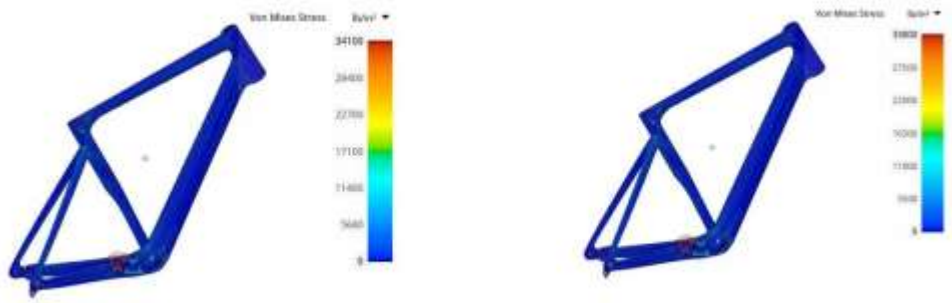

(a) Low carbon steel & (b) Aluminum alloy Von Mises Stresses induced in Bicycle frame in Case 2

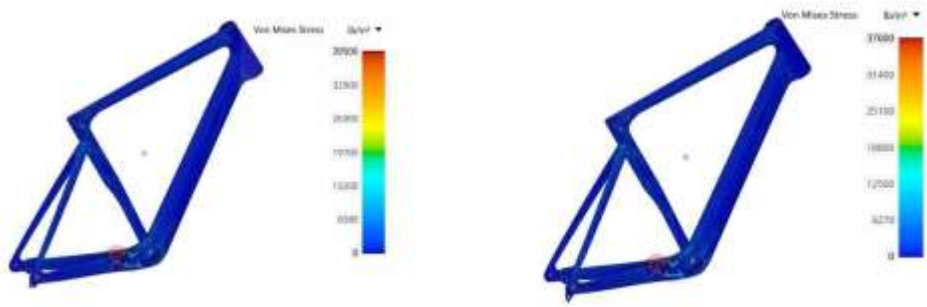

(c) CFRP & (d) GFRP Von Mises Stresses induced in Bicycle frame in Case 2

Fig. 5. Von Mises stress contours, Case 2 (incline): (a) steel, (b) aluminum 6061, (c) CFRP, (d) GFRP.

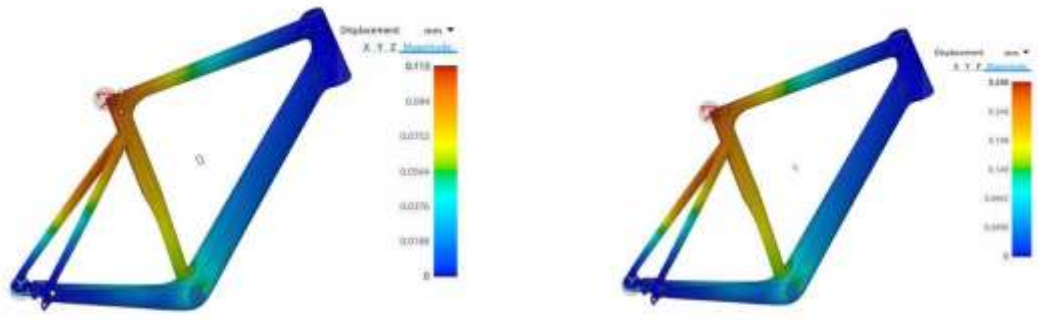

(a) Low carbon steel & (b) Aluminum alloy Total Displacement induced in Bicycle frame in Case 3

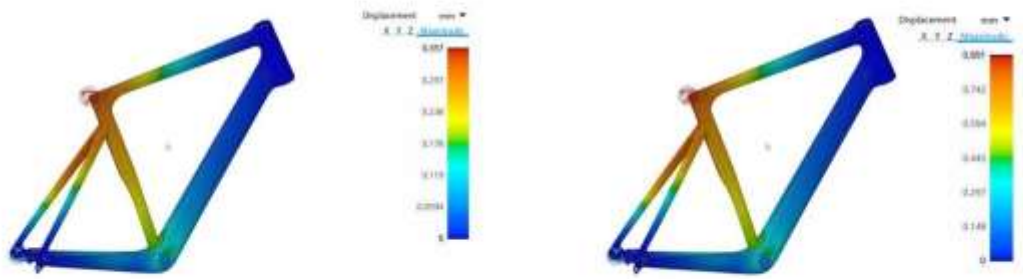

(c) CFRP & (d) GFRP Total Displacement induced in Bicycle frame in Case 3

Fig. 6. Total deformation contours, Case 3 (cornering): (a) steel, (b) aluminum 6061, (c) CFRP, (d) GFRP.

Comparing peak stress to yield strength (Table 1) gives an approximate static safety margin for each material and case; these ratios are derived here from the reported values and were not stated in the source thesis, following the same yield-strength-based safety-coefficient approach used by Şengül and Çalışkan [11] for a steel ramp structure. In Case 2 (incline), the most severe static scenario, the margins are: steel 430/235.11 = 1.83; aluminum 300/227.52 = 1.32; CFRP 1600/272.34 = 5.87; and GFRP 200/259.24 = 0.77. For the two metallic materials (steel, aluminum), a margin below 1.0 would indicate that the predicted Von Mises stress exceeds the yield strength, and this criterion is a standard, appropriate check for isotropic metals. For the two polymer composites (CFRP, GFRP), however, a Von Mises/yield-strength comparison is only a rough proxy: composite failure is governed by fiber/matrix-specific mechanisms (fiber breakage, matrix cracking, delamination) that Von Mises stress does not capture, and a rigorous assessment would require a composite-specific criterion such as Tsai–Hill, Tsai–Wu, or Hashin, none of which was applied in the source thesis or in this manuscript. With that caveat stated explicitly, the margin computed here for GFRP in Case 2 (0.77, i.e., predicted stress 259.24 MPa against a reported yield strength of 200 MPa; Table 1) is still a signal worth flagging rather than dismissing: it directly contradicts the blanket claim, present in related project documentation, that all four materials remained within allowable stress limits under every load case examined. This finding is carried forward into Section 4.4 and Section 5 as a preliminary, metal-failure-criterion-based observation - not a validated composite failure prediction - pending a proper composite failure analysis.

4.2. Dynamic Structural Response

Table 4 summarizes the case-level time-domain dynamic simulation results in MSC Adams. Under the heavier 1500 N load case, CFRP exhibits the highest dynamic stress (120 MPa), exceeding steel (75.15 MPa)

and aluminum (73 MPa). Under the lighter 900 N load case, CFRP's stress drops sharply to 33 MPa, while steel, aluminum, and GFRP report unchanged values from the 1500 N case. This indicates that, in the case-level data, CFRP's dynamic stress response is considerably more load-sensitive than that of the other three materials - though the fact that steel, aluminum, and GFRP report identical stress values across two different applied loads (1500 N vs. 900 N) is itself unusual and is flagged as a possible modeling or reporting artifact in Section 5 rather than presented as a confirmed physical result.

Table 4. Dynamic structural results — MSC Adams time-domain simulation, reported by load case.

Material	Case 1 (1500 N) Stress (MPa)	Case 1 Deformation (mm)	Case 2 (900 N) Stress (MPa)	Case 2 Deformation (mm)
Low-Carbon Steel	75.15	0.21	75.15	0.11
Aluminum Alloy 6061	73.00	0.29	73.00	0.29
CFRP	120.00	0.33	33.00	0.22
GFRP	82.00	0.89	82.00	0.89

A second summary table in the source thesis (its own "overall static/dynamic comparison") reports different dynamic Von Mises stress values - steel 160 MPa, aluminum 165.64 MPa, CFRP 120 MPa, and GFRP 173 MPa - shown in Table 5 for completeness. The CFRP value (120 MPa) agrees with the case-level Table 4, but the steel, aluminum, and GFRP values do not, and the source material gives no basis for reconciling the two. Per the instruction to surface rather than silently resolve such conflicts, both tables are reported here, and this discrepancy is treated as an open item requiring verification against the original MSC Adams simulation files before the dynamic-stress comparison can be considered final.

Table 5. Overall static vs. dynamic comparison, reproduced from the source thesis, with both reported dynamic-stress datasets shown side by side (see discrepancy discussion above).

Material	Static Stress (MPa)	Dynamic Stress - case-level (MPa)	Dynamic Stress - overall-comparison table (MPa)	Static Deformation (mm)	Dynamic Deformation (mm)
Low-Carbon Steel	170.98	75.15	160.00	0.19	0.11
Aluminum Alloy 6061	170.30	73.00	165.64	0.49	0.29
CFRP	169.60	120.00	120.00	0.84	0.33
GFRP	168.92	82.00	173.00	1.47	0.89

4.3. Comparative Material Performance

Specific stiffness (E/ρ) and specific strength (σy/ρ), calculated directly from Table 1, provide a weight-normalized comparison not reported explicitly in the source thesis:

Table 6. Specific stiffness and specific strength, derived from Table 1 (E/ρ and yield strength/ρ).

Material	Specific Stiffness, E/ρ (GPa per Mg/m³)	Specific Strength, σy/ρ (MPa per Mg/m³)
Low-Carbon Steel	26.9	53.8
Aluminum Alloy 6061	25.0	107.1
CFRP	137.4	879.1
GFRP	16.7	111.1

CFRP leads both metrics by a wide margin - roughly five times steel's specific stiffness and over sixteen times its specific strength - which is consistent with CFRP's favorable dynamic load-sensitivity in Table 4 and with the electric-bike findings of Iskandar et al. [8], who also identified carbon fiber as the best-performing

material on a strength/stiffness/weight basis, albeit for a different frame and loading context. Aluminum alloy shows the lowest static Von Mises stress overall while giving moderately higher deformation than steel; steel gives comparatively low deformation but at a significant weight penalty (density 7990 kg/m³, roughly 2.9× aluminum and 4.4× CFRP/GFRP). A material factor likely affecting the composite results is that CFRP and GFRP were represented in the FEA using bulk isotropic properties (Table 1) rather than a true ply-by-ply anisotropic laminate; this simplification, noted explicitly as future work in the source project, likely understates the composites' true directional stiffness and may partly explain why CFRP recorded the largest static deformation of the four materials in Case 1 despite its high specific stiffness.

4.4. Engineering Implications

Three application-driven material strategies follow from the results. For lightweight, high-performance builds, CFRP offers the best specific-stiffness and specific-strength performance (Table 6) and the best dynamic load-sensitivity (Table 4), at higher manufacturing cost and complexity, and with the isotropic-modeling caveat above. For balanced performance and cost, aluminum alloy 6061 gives the lowest static stress among the four materials and a moderate weight penalty, though it remains susceptible to fatigue - a concern this static/dynamic study does not itself evaluate (Section 5). For cost-conscious, general-purpose builds, low-carbon steel remains the most affordable, most predictable, and most readily manufactured option, with comparatively low deformation but the highest mass. These positions are consistent with the qualitative comparison in Table 1b: steel is rated lowest in manufacturing complexity and cost but only moderate in fatigue resistance and weight-to-strength ratio, while CFRP is rated highest in cost and manufacturing complexity but also in corrosion resistance, fatigue resistance, and weight-to-strength ratio - reinforcing that the CFRP/steel choice is a genuine trade-off rather than a case where one material dominates on every criterion. GFRP warrants caution for incline-heavy riding: its predicted Case 2 Von-Mises stress exceeds its own yield strength by the metal-appropriate criterion used in Section 4.1 (Table 1), and it also produced the largest deformation of the four materials in every static case examined. Because yield strength is not, strictly, the correct failure criterion for a composite, this is reported as a flag rather than a confirmed failure prediction - but it is a flag that a purely qualitative reading of the source project's conclusions (which favor “carbon fiber” generally, without distinguishing CFRP from GFRP) would not surface, and it should be verified with a composite-specific failure criterion and the original ANSYS model before being used for design guidance.

5. Limitations

The following limitations apply to the analysis reported in the source thesis and are carried forward here rather than omitted:

- Numerical (FEA and multibody simulation) rather than experimental validation - no physical strain-gauge or modal-hammer testing was performed.
- CFRP and GFRP were modeled using bulk isotropic material properties rather than a ply-by-ply anisotropic laminate, likely understating their true directional stiffness.
- Mesh element/node counts and a formal mesh-convergence study are not reported in the source thesis [information required].
- Two internal inconsistencies in the source data are unresolved: (a) the case-level dynamic-stress table and the overall-comparison table report different dynamic stress values for steel, aluminum, and GFRP (Section 4.2); and (b) the source project's claim that all materials remained within allowable stress limits is contradicted by GFRP's Case 2 static stress exceeding its own yield strength (Section 4.1). Both should be verified against the original ANSYS Discovery and MSC Adams model files before publication.
- Static load cases use simplified rigid tilt angles (15°) with a single rider load point and linear-elastic material behavior; no fatigue analysis, manufacturing-defect modeling, or rider/environment interaction beyond gravity and applied point loads was performed.
- The static boundary conditions fix the rear dropout and bottom bracket rigidly. This is a common simplification in frame FEA, but it does not fully represent real riding conditions - in practice the rear dropout

and bottom bracket are not rigid supports but are themselves connected to a compliant drivetrain, wheel, and ground contact - and the reported stress distribution should be understood as being shaped in part by this modeling choice rather than purely by material and geometry.

• CFRP and GFRP results are evaluated in Section 4.1 using a yield-strength/Von-Mises-stress margin, which is a standard criterion for isotropic metals but only an approximate proxy for composites; a rigorous assessment would require a composite-specific failure criterion (e.g., Tsai–Hill, Tsai–Wu, or Hashin), none of which was available in the source data.

• The method used to derive structural Von Mises stress and deformation from the MSC Adams multibody simulation (e.g., Adams/Flex vs. a coupled external FEA solver) is not stated in the source thesis and is marked [information required] in Section 3.6; this affects how much confidence can be placed in the absolute dynamic-stress values in Section 4.2.

• No formal modal (natural-frequency) analysis was performed, despite being listed as a project objective; the dynamic results reported here are time-domain multibody results, not modal results.

• In the case-level dynamic table, steel, aluminum, and GFRP report identical Von Mises stress values under two different applied loads (1500 N and 900 N), which is not explained in the source thesis and may indicate a modeling or reporting artifact rather than confirmed physical insensitivity to load.

6. Conclusions

This study compared four candidate bicycle-frame materials - low-carbon steel, aluminum alloy 6061, CFRP, and GFRP - using static FEA (ANSYS Discovery, three load cases) and time-domain multibody dynamic simulation (MSC Adams, two load cases) on a common sixteen-part CAD frame model. Under straight-line static riding, stress was nearly material-independent (within about 1.3%) while deformation varied roughly eightfold across materials, confirming that stress in this geometry is governed chiefly by load path while deformation is governed by material stiffness. In the dynamic simulation's case-level data, CFRP showed the greatest load sensitivity, with stress falling from 120 MPa to 33 MPa between the 1500 N and 900 N cases; this observation should be treated as preliminary rather than conclusive, since the method used to derive stress from the Adams multibody model is not documented in the source data (Section 3.6) and a second source table reports different dynamic-stress values for the other three materials (Section 4.2). The most consequential trade-off identified is that CFRP and aluminum offer the best specific-stiffness and specific-strength performance for weight-sensitive builds, steel remains the most predictable and cost-effective general-purpose option, and GFRP - despite lower cost than CFRP - shows a Von-Mises-stress margin below its yield strength in the 15° incline case; because this margin uses a metal-appropriate criterion rather than a composite-specific one (Tsai–Hill, Tsai–Wu, or Hashin), it is reported here as a flag warranting further composite-specific analysis rather than a confirmed failure prediction. The overarching engineering implication is that frame-material selection should be driven by application priorities (performance, affordability, and terrain profile) rather than by a single materials-wide recommendation, and that the specific numerical comparisons in this study should be read as preliminary pending the outstanding verification items below. Recommended future work includes a mesh-convergence study with reported element/node counts, complete frame geometric specifications (tube diameters, wall thicknesses, angles), formal modal analysis, fatigue and life-cycle prediction under repeated loading, ply-by-ply anisotropic laminate modeling of CFRP/GFRP with composite-specific failure criteria, documentation of the Adams stress-extraction method, experimental validation (e.g., strain-gauge or modal testing) against the numerical results, physical prototype validation, and reconciliation of the dynamic-stress table discrepancy identified in Section 4.2.

Author Contributions

Conceptualization, methodology, software, validation, formal analysis, investigation, data curation, and writing - original draft, S.K.; supervision, project administration, and writing - review and editing, S.A.S. All authors have read and agreed to the published version of the manuscript.

Funding
This research received no external funding.

Data Availability Statement
The data presented in this study are derived from the corresponding author's MSc thesis ["Static & Dynamic Simulation of Bicycle Frame using Finite Element Analysis," University of Engineering and Technology, Peshawar, 2023]. The underlying ANSYS Discovery and MSC Adams model files were not available for re-verification at the time of manuscript preparation; see Section 5 for the resulting limitations.

Acknowledgments
The authors thank the Department of Mechanical Engineering, University of Engineering and Technology, Peshawar, for providing the resources and facilities necessary to complete this work.

Conflicts of Interest
The authors declare no conflicts of interest.

References

1. Heinen, E., Van Wee, B., & Maat, K. (2010). Commuting by bicycle: An overview of the literature. *Transport reviews*, *30*(1), 59-96.
2. Collins, P. K., Leen, R., & Gibson, I. (2016). Industry case study: rapid prototype of mountain bike frame section. *Virtual and Physical Prototyping*, *11*(4), 295-303.
3. Devaiah, B.B.; Purohit, R.; Rana, R.S.; Parashar, V. (2018) Stress Analysis of a Bicycle Frame. Mater. Today Proc.5, 18920–18926.
4. Callens, A.; Bignonnet, A. (2012). Fatigue design of welded bicycle frames using a multiaxial criterion. Procedia Eng., 34, 640–645.
5. Maleque, M.A.; Hossain, M.S.; Dyuti, S. (2011). Material Properties and Design Aspects of Folding Bicycle Frame. Adv. Mat. Res., 264–265, 777–782.
6. Ayachi, F.S.; Dorey, J.; Guastavino, C. (2015). Identifying factors of bicycle comfort: An online survey with enthusiast cyclists. Appl. Ergon. 46, 124–136.
7. Schwab, A.L.; Meijaard, J.P. (2013). A review on bicycle dynamics and rider control. Veh. Syst. Dyn. 51, 1059–1090.
8. Iskandar, R.; Sawitri, D.; Hantoro, R.; Zulkifli, I.; Pratama, Y. (2021). Analysis of dynamics mechanical properties of electric bike frames using finite element analysis (FEA). AIP Conf. Proc. 2384, 070005.
9. Sani, M.S.M.; Nazri, N.A.; Zahari, S.N.; Abdullah, N.A.Z.; Priyandoko, G. (2016). Dynamic Study of Bicycle Frame Structure. IOP Conf. Ser. Mater. Sci. Eng, 160, 012009.
10. Evran, S.; Kurt, M. (2024). Numerical evaluation of material type on topology optimization of thin square plates. J. Mater. Manuf. 3, 1–7.
11. Şengül, O.; Çalışkan, F. (2024). Design and FEM analysis of hatch ramps for sea freight transport. J. Mater. Manuf. 3, 18–31.